Measurements of absolute line strength of the $\nu 1$ fundamental transitions of OH radical and rate coefficient of the reaction OH + H2O2 with mid-infrared two-color time-resolved dual-comb spectroscopy

Che-Wei Chang, I-Yun Chen, Christa Fittschen, Pei-Ling Luo

Accepted to J. Chem. Phys. 10.1063/5.0176311

The Journal of Chemical Physics

AIP Publishing

Measurements of absolute line strength of the v_1 fundamental transitions of OH radical and rate coefficient of the reaction OH + H_2O_2 with mid-infrared two-color time-resolved dual-comb spectroscopy

Che-Wei Chang,[1] I-Yun Chen,[1,2] Christa Fittschen,[3] and Pei-Ling Luo[1]*

[1] Institute of Atomic and Molecular Sciences Academia Sinica, Taipei 106319, Taiwan.

[2] Department of Chemistry, National Taiwan University, Taipei 106319, Taiwan.

[3] University Lille, CNRS, UMR 8522, PC2A–Physicochimie des Processus de Combustion et de l'Atmosphère, F-59000 Lille, France.

*corresponding author: plluo@gate.sinica.edu.tw

ABSTRACT:

Absolute line strengths of several transitions in the ν_1 fundamental band of the hydroxyl radical (OH) have been measured by simultaneous determination of the hydrogen peroxide (H_2O_2) and OH upon laser photolysis of H_2O_2. Based on the well-known quantum yield for generation of the OH radical in the 248-nm photolysis of H_2O_2, the line strength of the OH radicals can be accurately derived by adopting the line strength of the well-characterized transitions of H_2O_2 and analyzing difference absorbance time traces of H_2O_2 and OH obtained upon laser photolysis. Employing a synchronized two-color dual-comb spectrometer, we measured high-resolution time-resolved absorption spectra of the H_2O_2 near 7.9 μm and the OH radical near 2.9 μm, simultaneously, under varied conditions. In addition to studies of the line strengths of the selected H_2O_2 and OH transitions, the kinetics of the reaction between OH and H_2O_2 were investigated. A pressure-independent rate coefficient $k_{OH+H2O2}$ was determined to be [1.97 (+0.10 / –0.15)] × 10^{-12} cm^3 $molecule^{-1}$ s^{-1} at 296 K and compared with other experimental results. By carefully analyzing both high-resolution spectra and temporal absorbance profiles of H_2O_2 and OH, the uncertainty of the obtained OH line strengths can be achieved down to <10% in this work. Moreover, the proposed two-color time-resolved dual-comb spectroscopy provides a new approach for directly determining the line strengths of transient free radicals and holds promise for investigations on their self-reaction kinetics as well as radical–radical reactions.

I. INTRODUCTION

Being the most important oxidizing agent in the troposphere, the hydroxyl radical (OH) plays a crucial role to scavenge air pollutants and to influence the formation of atmospheric acids.[1–4] In both field measurements and laboratory studies, quantitative determination of the OH radical is essential to decipher the complex oxidation chain reactions as well as to evaluate the oxidizing capacity in the environments.[5,6] In most of experiments and field observations, the OH radical is detected by monitoring its $A^2\Sigma^+ - X^2\Pi$ electronic transitions with laser-induced fluorescence spectroscopy.[7–9] Although the laser-induced fluorescence detection is extremely sensitive for probing the OH radical, it requires additional calibrations to convert the fluorescence signals into absolute concentrations and the calibration accuracy might be affected by the fluorescence quenching effects and interferences of other species in the chamber.[10,11] Recently, several modern spectroscopic techniques have been proposed to detect the OH radical based on infrared absorption spectroscopy.[12–18] For instance, the OH overtone transitions $X^2\Pi_{1/2}$ (2←0) R(0.5)e and R(0.5)f have been measured by utilizing cw cavity ring-down spectroscopy near 7028 cm^{-1} and used for studing the kinetics of the reaction between OH and HO_2 radicals.[12] Furthermore, thanks to the development of the mid-infrared laser techniques, various methods such as 2f-IR wavelength modulation spectroscopy,[13] mid-infrared Faraday rotation spectroscopy,[14,15] optical-feedback cavity-enhanced absorption spectroscopy[16] and time-resolved dual-comb spectroscopy[17,18] have been demonstrated to detect the OH radiclas through probing its ν_1 fundamental transitions in the spectral range of 3400−3600 cm^{-1}. With rotationally resolved infrared absorption spectroscopy, line strengths of the selected transitions are significant and indispensable to obtain the concentrations of the OH

radicals. Currently, the line strengths of the OH transitions tabulated in the HITRAN database were derived based on theoretical simulations and near-infrared emission spectra of the OH Meinel bands observed from the Earth's atmosphere.[19–21] Direct line strength measurements of the OH fundamental transitions under well-controlled experimental conditions thus would be essential and important to confirm the accuracy of the simulated values from the HITRAN database and it might be also significant for various applications using mid-infrared absorption spectroscopy to quantify the OH radicals during reaction processes and in field investigations.

Here, we report direct measurements of line strengths of the OH ν_1 transitions via simultaneous determination of H_2O_2 and OH in the 248-nm photolysis of H_2O_2 reaction system. By employing two sets of dual-comb spectrometers near 7.9 and 2.9 μm, high-resolution time-resolved spectra of H_2O_2 and OH can be simultaneously recorded before and after laser photolysis of the flowing mixtures of H_2O_2/N_2 under different experimental conditions. In addition to first measuring the line strength of several ν_6 fundamental transitions of H_2O_2 in the region 1269.3−1269.7 cm^{-1}, the rate coefficients of the reaction OH + H_2O_2 were also accurately determined. The absolute line strengths of ten selected transitions in the OH ν_1 fundamental band were evaluated and comparable with simulated values from the HITRAN database.

II. EXPERIMENTAL METHODS

Herein, the OH radical can be produced by photolysis of H_2O_2 at 248 nm and it would further react with H_2O_2 to form H_2O and HO_2 radicals. According to the quantum yield ($\Phi = 2$) for generation of the OH radical in the 248-nm photolysis of H_2O_2,[22,23] the line strength of the OH transitions can be derived by the formula:

$$S_{OH} = -S_{H2O2} \times \frac{[\text{Int. } \Delta\text{Abs.}]_{OH,t=0}}{2\times[\text{Int. } \Delta\text{Abs.}]_{H2O2,t=0}} \quad (1)$$

where S_{H2O2} represents the line strength of H_2O_2. $[\text{Int. } \Delta\text{Abs.}]_{OH,t=0}$ and $[\text{Int. } \Delta\text{Abs.}]_{H2O2,t=0}$ represent the integrated difference absorbance areas of the OH and H_2O_2 absorption lines, respectively, obtained right at flash photolysis.

To determine the line strength of H_2O_2 and the ratios of the integrated difference absorbance areas of the OH and H_2O_2 upon flash photolysis, we operated two sets of dual-comb systems with central wavelengths near 2.9 and 7.9 μm and a Herriott-type multipass reactor cell which was designed with a total multipass length of 41.8 m. Figure 1 shows the schematic of the experimental setup for measurements of line strengths of the ν_1 fundamental transitions of OH radicals. To generate the OH radicals, we performed photolysis of the flowing mixtures of H_2O_2/N_2 with an excimer laser at 248 nm. A stable and water-free source of gaseous H_2O_2 was used and it can be produced by employing thermal decomposition of the H_2O_2−urea complex. In the experiment, the gaseous H_2O_2 was generated by heating a mixture of H_2O_2−urea with SiO_2 to ~40 °C and then it was carried by a stream of nitrogen into a 50-cm UV absorption cell, before being introduced to the multipass cell. The mixing ratio of the H_2O_2/N_2 mixtures before injection into the multipass cell was evaluated by employing the measured UV absorption spectra and the absorption cross section of H_2O_2 in region 215–220 nm. The mirrors and windows of the

multipass cell were purged by streams of nitrogen. Each stream of nitrogen was controlled by the calibrated mass flow controller. The pressures of the UV absorption cell and the multipass cell were measured with the absolute pressure gauges. The partial pressure of the precursor H_2O_2 in the multipass cell hence can be calculated using the flow rate of each stream, mixing ratios of the H_2O_2/N_2 pre-mixtures, and the total pressure of the multipass cell. The temperature in the experimental environment was controlled at (296 ± 0.5) K and the temperature in the chamber can be monitored using a common thermometer. The wavelength-tunable dual-comb sources were constructed using difference frequency generation between the near infrared electro-optic comb systems and widely tunable cw lasers.[24,25] In this work, the reaction species H_2O_2 and OH in the multipass cell were probed by the 7.9 and 2.9-μm dual-comb sources, respectively. After passing through the multipass absorption cell, each dual-comb source was detected with the HgCdTe photodiode and the time-dependent dual-comb interferograms were recorded with the data acquisition board to further obtain the time-dependent transmission spectra of H_2O_2 and OH via Fourier transformation. To clearly evaluate the spectral variations after flash photolysis as well as to reduce the spectral noise caused from laser sources, the time-dependent difference absorbance ($[\Delta Abs.]_t$) spectra were employed for analysis of the time traces of H_2O_2 and OH and they can be derived by the formula:

$$[\Delta Abs.]_t = [Abs.]_t - [Abs.]_i = -\ln[\frac{T_t(\nu)}{T_i(\nu)}] \quad (2)$$

where $T_i(\nu)$ and $T_t(\nu)$ are the transmission spectra obtained respectively before and after flash photolysis. $[Abs]_i = -\ln[T_i(\nu)]$ represents the precursor absorbance spectrum taken before photolysis and $[Abs.]_t = -\ln[T_t(\nu)]$ represents the time-dependent absorbance

spectra taken after photolysis. The data processing method of high-resolution time-resolved dual-comb spectroscopy was described in our previous works.[17,18]

Figure 2 displays the representative time-resolved dual-comb spectra obtained upon the 248-nm irradiation of a flowing mixture of H_2O_2/N_2 (0.0145/10.04 Torr, P_T = 10.05 Torr, 296 K) over 5000 excimer laser shots. The initial absorbance and the depletion of H_2O_2 caused by flash photolysis and the reaction of OH + H_2O_2 can be evaluated by measuring several ν_6 fundamental transitions of H_2O_2 in the region of 1269.3–1269.7 cm^{-1}, as shown in Figure 2(a). In addition, the formation and sink of OH radicals in the reaction system can be simultaneously observed by probing the selected ν_1 fundamental transitions such as the $X^2\Pi_{1/2}$ (1←0) P(3.5) doublet lines in the region of 3421.88–3422.08 cm^{-1}, as displayed in Figure 2(b). With our experimental system, the noise floor of the difference absorbance profile (e.g., Figure S2) extracted from the time-resolved dual-comb spectra (Figure 2(b)) can be estimated down to ~2×10^{-4}. The spectral sampling points of the time-resolved dual-comb spectra can be increased by interleaving multiple measurements with different spectral sampling spacings and the time resolution can be adjusted from tens of μs to a few ms, according to the acquisition time of dual-comb interferogram used for generation of each time-dependent difference absorbance spectrum.

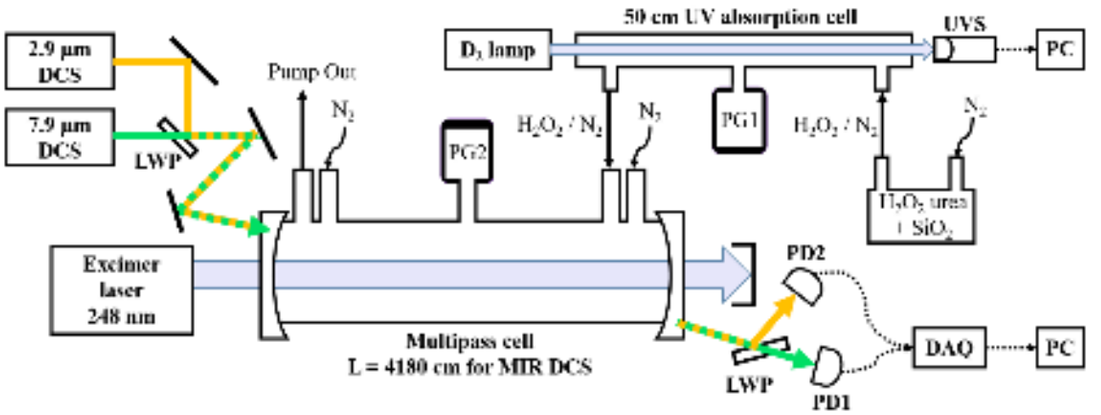

FIGURE 1. Schematic of the experimental setup. Here, DCS is the dual-comb source, LWP is the longwave pass filter, PG is the pressure gauge, PD is the photodiode, DAQ is the data acquisition board, UVS is the ultraviolet spectrometer, and PC is the personal computer.

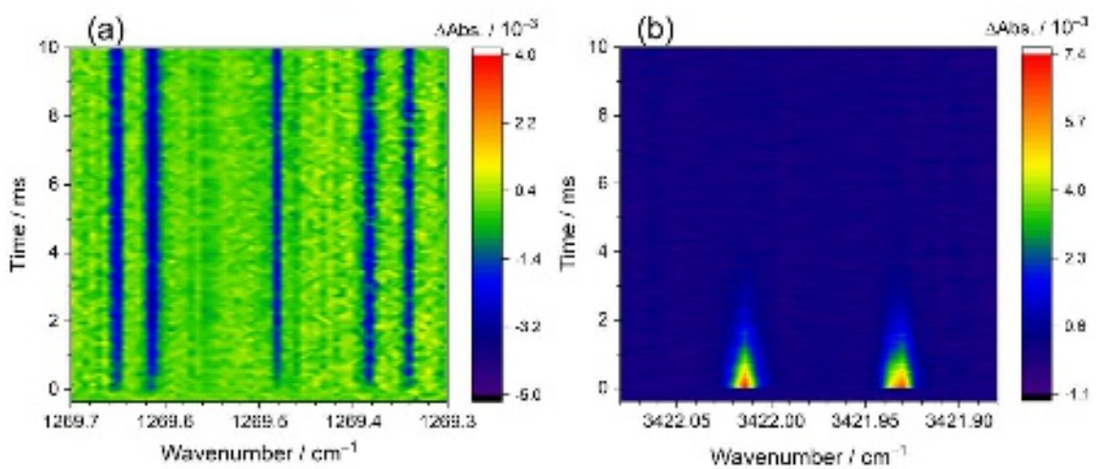

FIGURE 2. Representative time-resolved dual-comb spectra in the regions (a) 1269.3–1269.7 cm^{-1} and (b) 3421.88–3422.08 cm^{-1}. The spectra were recorded simultaneously upon the 248-nm irradiation of a flowing mixture of H_2O_2/N_2 (0.0145/10.04 Torr, P_T = 10.05 Torr, 296 K) over 5000 excimer laser shots. Here, the spectral sampling spacing is 210 MHz (7×10^{-3} cm^{-1}). The temporal resolutions of (a) and (b) are set to be 100 and 40 μs, respectively.

III. RESULTS AND DISCUSSION

A. Line strength measurements of the ν_6 fundamental transitions of H_2O_2 near 7.9 μm.

To determine the absolute line strength of the ν_6 fundamental transitions of H_2O_2 in the region of 1269.3–1269.7 cm^{-1}, the interleaved dual-comb spectra were recorded with spectral sampling spacings of 151, 181, and 210 MHz and fitted using a multi-peak Voigt function to obtain the integrated absorbance areas of the six absorption peaks (P1, P2, P3, P4, P4', and P5), as shown in Figure 3. The line strength of each peak can be derived by the formula:

$$S_{H2O2} = \frac{[\text{Int. Abs.}]_{H2O2}}{[H_2O_2]\times L} \quad (3)$$

where S_{H2O2} represents the line strength of H_2O_2, $[\text{Int. Abs.}]_{H2O2}$ represents the integrated absorbance area of the absorption peak of H_2O_2, $[H_2O_2]$ is the concentration of H_2O_2 obtained in the multipass cell, and L is the total absorption length for dual-comb beam. To accurately determine the concentration of H_2O_2 inside the multipass cell and to make sure that no loss of H_2O_2 was caused during flowing, we used two set of UV absorption spectrometers to measure the mixing ratios of the H_2O_2/N_2 mixtures before flowing into the multipass cell and after passing through the cell. The concentration of H_2O_2 in the UV absorption cell can be obtained according to the measured UV absorption spectra and the integrated absorption cross-sections of H_2O_2 for the range 215−220 nm ($\sigma_{215-220nm}$) derived from previous experimental measurements (Figure S1).[26–29] Considering the errors of the $\sigma_{215-220nm}$ (4%), flow rates (1%), temperature (1%), and pressure (3%), the $[H_2O_2]$ can be determined with an overall uncertainty of 5.2%. Over 11 measurements were carried out at experimental conditions with $[H_2O_2]$ = (8.6–19.7) × 10^{13} molecules cm^{-3} and total pressure P_T = 8.95–10.42 Torr at 296 K. The plots of the obtained integrated absorbance

areas [Int. Abs.]$_{H2O2}$ against the [H_2O_2] for each absorption peak are shown in Figure S3. The peak strength hence can be derived through dividing the fitted slope of each plot of the [Int. Abs.]$_{H2O2}$ versus [H_2O_2] by the total absorption path. The overall uncertainty, including the errors of the fitted slope (1.2%), concentration of H_2O_2 (5.2%), and absorption path (1.4%), was estimated to be 5.5%. Table 1 shows a comparison of the measured line strengths of the absorption peaks of H_2O_2 with the values tabulated in the HITRAN database.[21] The current HITRAN data for the line strengths of the H_2O_2 ν_6 band was derived according to previous FTIR measurements and the uncertainty of the line strength of the ν_6 band in H_2O_2 was reported to be ~10%.[30] The line strengths of the absorption peaks P1 and P5 were obtained in agreement with the HITRAN values. For the P2 and P2', the summed line strength was found slightly lower, but it was still comparable with that from HITRAN database. By contrast, a discrepancy between the obtained peak strengths and the values from HITRAN database for the P3, P4 and P4' was observed because there are several hot torsion–vibration transitions of the H_2O_2 ν_6 band nearby and these line positions and strengths might be not accurate in the HITRAN simulation.[31] To avoid the possible uncertainty from these hot torsion–vibration transitions in subsequent experiments, we mainly analyzed the time-dependent difference absorbance spectra in the spectral range of 1269.57–1269.70 cm^{-1} and the spectra of the absorption peak P5 to explore the depletion of H_2O_2 caused by UV photolysis and the reaction of OH + H_2O_2 as well as to further determine the absolute line strength of the OH ν_1 transitions.

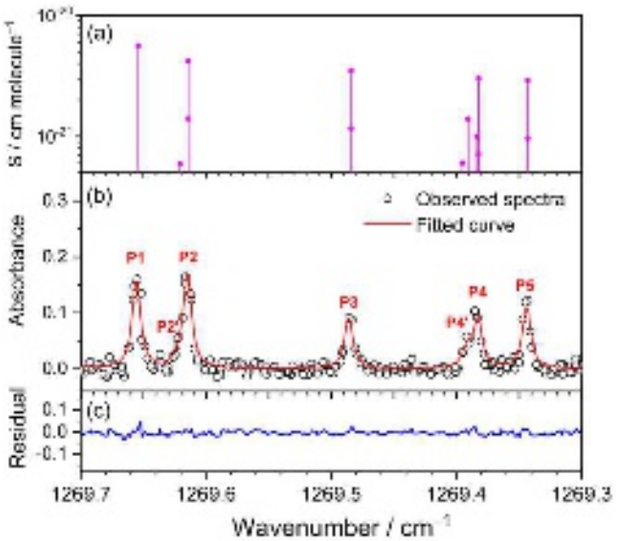

FIGURE 3. (a) The transition lines of H_2O_2 taken from HITRAN database. (b) The observed dual-comb spectra and the fitted curve. (c) The fitting residual. Here, the spectra were measured using a 41.8-m multi-pass cell with a flowing mixture of H_2O_2/N_2 (0.00264/10.42 Torr, P_T = 10.42 Torr, 296 K). The observed spectra were fitted using a multi-peak Voigt function to obtain the integrated absorbance areas of the seven absorption peaks (P1, P2, P2', P3, P4, P4', and P5).

TABLE 1. Comparison of the obtained line strengths of the H_2O_2 peaks with the values tabulated in the HITRAN database.

Peak	Line center [a] /cm^{-1}	Transition [a]	Line strength [a,b,c]	HITRAN Peak strength [b,c,d]	Observed peak strength [b,e]	Difference [f]
P1	1269.654	ν_6 (0,1)$3_{0,3}$ ←$2_{0,2}$	5.58×10^{-21}	5.58×10^{-21}	5.29×10^{-21}	−5.2%
P2 & P2'	1269.621	ν_6 (2,2)$9_{5,4}$ ←$10_{5,5}$	5.91×10^{-22}	6.38×10^{-21}	5.38×10^{-21}	−15.7%
	1269.621	ν_6 (2,2)$9_{5,5}$ ←$10_{5,6}$	1.97×10^{-22}			
	1269.614	ν_6 (0,1)$11_{6,5}$ ←$11_{6,6}$	1.40×10^{-21}			
	1269.614	ν_6 (0,1)$11_{6,6}$ ←$11_{6,5}$	4.19×10^{-21}			
P3	1269.484	ν_6 (0,1)$12_{6,6}$ ←$12_{6,7}$	3.49×10^{-21}	4.65×10^{-21}	3.11×10^{-21}	−33.1%
	1269.484	ν_6 (0,1)$12_{6,7}$ ←$12_{6,6}$	1.16×10^{-21}			
P4 & P4'	1269.395	ν_6 (2,4)$15_{2,14}$ ←$16_{2,15}$	6.03×10^{-22}	7.18×10^{-21}	4.19×10^{-21}	−41.6%
	1269.391	ν_6 (2,2)$8_{3,6}$ ←$9_{3,7}$	1.39×10^{-21}			
	1269.391	ν_6 (2,2)$8_{3,5}$ ←$9_{3,6}$	4.62×10^{-22}			
	1269.384	ν_6 (1,4)$4_{2,3}$ ←$5_{2,4}$	1.00×10^{-21}			
	1269.382	ν_6 (2,3)$15_{1,14}$ ←$16_{1,15}$	7.13×10^{-22}			
	1269.382	ν_6 (1,4)$4_{2,2}$ ←$5_{2,3}$	3.01×10^{-21}			
P5	1269.343	ν_6 (0,1)$13_{6,7}$ ←$13_{6,8}$	9.66×10^{-22}	3.87×10^{-21}	3.59×10^{-21}	−7.2%
	1269.343	ν_6 (0,1)$13_{6,8}$ ←$13_{6,7}$	2.90×10^{-21}			

[a] Line parameters tabulated in the HITRAN database.[21]
[b] Strength in cm molecule^{-1}.
[c] The uncertainty of the line strength of the H_2O_2 ν_6 band from HITRAN database is ~10%.[30]
[d] Sum of the line strengths of the assigned transitions for each peak.
[e] The observed peak strength with an overall uncertainty of 5.5%.
[f] The difference is defined as (observed peak strength – HITRAN Peak strength) / (HITRAN Peak strength).

B. Determination of the rate coefficient for the reaction OH + H_2O_2.

To better evaluate the time-resolved difference absorbance spectra of both H_2O_2 and OH radicals, we first determine the rate coefficients of the reaction between OH and H_2O_2 by analyzing the temporal profiles of the OH absorption lines obtained under varied conditions. Over 34 measurements in six sets were conducted under the conditions with the estimated OH initial concentration $[OH]_0 \approx (2.7–3.9) \times 10^{12}$ molecules cm^{-3}, the determined H_2O_2 initial concentration $[H_2O_2]_0 = (3.15–9.22) \times 10^{14}$ molecules cm^{-3}, and the total pressure P_T = 10.1–55.0 Torr at 296 K. Because the depletion of H_2O_2 caused by 248-nm photodissociation with the employed energy of 19.0–42.8 mJ cm^{-2} was estimated to be only 0.22–0.48% and initial concentrations of H_2O_2 were greatly larger than that of OH radicals, herein we can perform the kinetic studies of the reaction OH + H_2O_2 under pseudo-first-order conditions. The decay in the concentration of the OH radicals with time hence can be described with a single-exponential formula:

$$[OH]_{obs}(t) = [OH]_0 \times \exp(-k_{obs} \times t) \quad (4)$$

in which $[OH]_{obs}(t)$ represents the observed concentration of the OH radicals as a function of time, $[OH]_0$ represents the initial concentration of OH generated right on flash photolysis, and k_{obs} indicates the overall decay rate coefficients of the observed OH time traces:

$$k_{obs} = k_0 + k_{OH+H2O2} \times [H_2O_2]_0 \quad (5)$$

where k_0 is the decay rate coefficient that might be contributed by the reaction of OH with HO_2, $k_{OH+H2O2}$ is the second-order rate coefficient of the reaction OH + H_2O_2, and $[H_2O_2]_0$ is the initial concentration of H_2O_2 obtained in the multipass reaction cell. Figure 4(a) shows the representative temporal profiles of the OH radicals obtained by probing the OH

$X^2\Pi_{3/2}$ (1←0) P(2.5)e transition near 3484.75 cm^{-1} with conditions using different $[H_2O_2]_0$ and photolysis energy. Each observed OH time trace (open symbol) was fitted with a single-exponential curve (solid line) to obtain the decay rate coefficient (k_{obs}), as displayed in Figure 4(b). The second-order rate coefficients $k_{OH+H2O2}$ can be derived from the linear fitted slopes of the plots of the k_{obs} against the $[H_2O_2]_0$. All experimental conditions and obtained k_{obs} are listed in Table S1. For each experimental set, the initial concentration of OH of each individual experiment was set to be the same by adjusting the adopted $[H_2O_2]_0$ and power of the photolysis laser. The obtained k_{obs} from the single-exponential fits as a function of $[H_2O_2]_0$ for the six experimental sets are displayed in Figure S4. Figure 5 shows the derived $k_{OH+H2O2}$ as a function of the total pressure at 296 K. Considering one standard deviation of the $k_{OH+H2O2}$ obtained from the six experimental sets (1%) and the error of determined $[H_2O_2]_0$ (5.2%), the overall uncertainty was estimated to be 5.3%. In addition, because the OH radicals can also react with HO_2 radicals generated from the reaction OH + H_2O_2 with the rate coefficients of (1–10) $\times 10^{-11}$ cm^3 $molecule^{-1}$ s^{-1} at 296 K,[12,32] herein we also analyzed the time traces of OH with a kinetic model which includes self-reactions of the OH and HO_2 as well as the radical-radical reaction OH + HO_2, as listed in Table S2. By employing the model fit with the k_{OH+HO2} = 1×10^{-11} cm^3 $molecule^{-1}$ s^{-1}, the derived second-order rate coefficients $k_{OH+H2O2}$ are the same as the values obtained using the single-exponential fit. In comparison, the $k_{OH+H2O2}$ obtained using the model fit with the faster k_{OH+HO2} = 1×10^{-10} cm^3 $molecule^{-1}$ s^{-1} are ~2.5% smaller than that from the single-exponential fit, as shown in Figure S4. By taking into account the overall statistic and systematic errors (5.3%) and the possible bias of –2.5% caused by the faster k_{OH+HO2}, the pressure independent $k_{OH+H2O2}$ was hence obtained to be [1.97 (+0.10 / –0.15)] $\times 10^{-12}$ cm^3

molecule^{-1} s^{-1} at 296 K. A comparison of the rate coefficients $k_{OH+H2O2}$ derived from different experiments with various methods and conditions is shown in Table 2. Currently, the recommended value of $k_{OH+H2O2}$ at 298 K from the evaluated kinetic and photochemical data for atmospheric chemistry (IUPAC) is 1.7×10^{-12} cm^3 molecule^{-1} s^{-1} and it was mainly derived based on the previous experiments in 1980s.[33] For these experiments, the $k_{OH+H2O2}$ were reported to be $(1.6-1.8) \times 10^{-12}$ cm^3 molecule^{-1} s^{-1} with the uncertainty of 8−20%.[34–39] In this work, the obtained rate coefficient $k_{OH+H2O2}$ is in excellent agreement with the more recent value reported by Jiménez *et al.*,[40] but it is 16% higher than that of the IUPAC preferred value.[33] Our work as an independent experiment that accomplished through direct measurements of the OH infrared absorption signals under well-controlled experimental conditions and using the new and water-free source of gaseous H_2O_2 as the precursor and reactant might play a crucial role to revisit the rate coefficient of the reaction OH + H_2O_2.

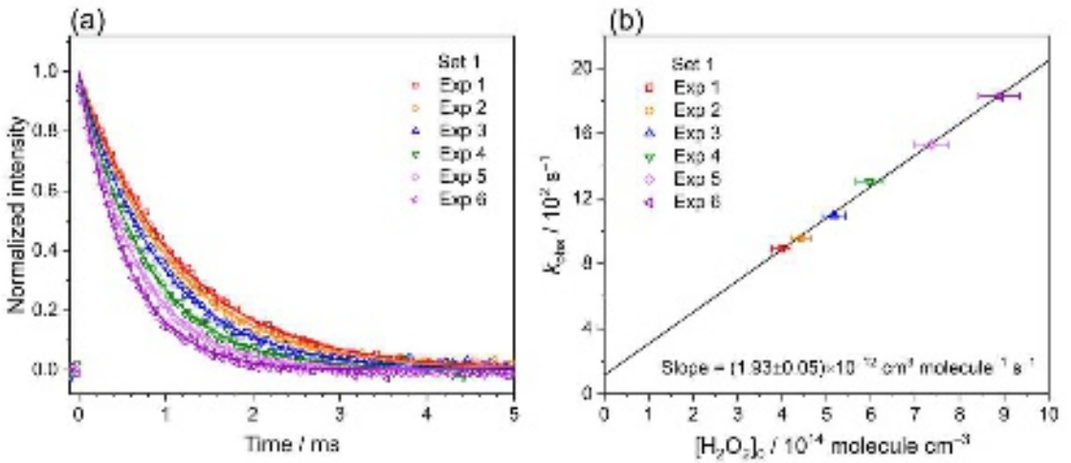

FIGURE 4. (a) Temporal profiles of the OH obtained under conditions with different $[H_2O_2]_0$ and photolysis energy. The open symbols represent experimental data recorded with the time resolution of 40 μs. The solid lines represent fitting curves. Each temporal profile was fitted with a single-exponential function to obtain the decay rate coefficient (k_{obs}). The data correspond to experiment 1–6 listed in Table S1 with total pressure P_T = 25.6 Torr, temperature 296 K, and $[OH]_0 \approx 3.9\times10^{12}$ molecule cm^{-3}. The derived k_{obs} as a function of $[H_2O_2]_0$ is shown in (b). The black line represents the linear fitting curve with a slope of $(1.93 \pm 0.05) \times 10^{-12}$ cm^3 molecule^{-1} s^{-1}

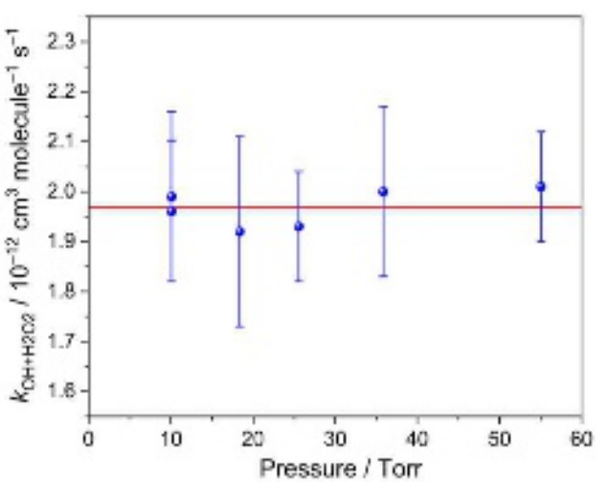

FIGURE 5. Rate coefficients for the reaction OH + H_2O_2 as a function of the total pressure. Each rate coefficient is the fitted slope of the plot of k_{obs} against $[H_2O_2]_0$ of each experimental set at 296 K. The error bars include the errors of the fitted slope and determined $[H_2O_2]_0$ and the red line represents the average value of the six experiment sets.

TABLE 2. Summary of experimental conditions, methods and results for determinations of the rate coefficient of the reaction OH + H_2O_2.

Study	Pressure / Torr	T / K	H_2O_2 source	OH generation method	OH detection method	$k_{OH+H2O2}$[a]
This work	10.1−55.0	296	Thermal decomposition of H_2O_2−urea complex	248-nm-photolysis of H_2O_2	IR absorption	$1.97\,^{+0.10}_{-0.15}$
Jiménez *et al.* [40] (2004)	13−16 / 100	298	95% (w/w) $H_2O_{2(aq)}$	193-nm-photolysis of H_2O_2	LIF[b]	2.00 ± 0.15
Vaghjiani *et al.*[34] (1989)	50–550	298	97% (w/w) $H_2O_{2(aq)}$	248-nm-photolysis of H_2O_2	LIF[b]	1.86 ± 0.18
Kurylo *et al.* [35] (1982)	20–30	296	40% (w/w) $H_2O_{2(aq)}$	165–180-nm-photolysis of H_2O_2	Resonance fluorescence	1.79 ± 0.14
Marinelli *et al.* [36] (1982)	10	298	90–98% (w/w) $H_2O_{2(aq)}$	248-nm-photolysis of H_2O_2	Resonance fluorescence	1.81 ± 0.24
Wine *et al.* [37] (1981)	100	297	90% (w/w) $H_2O_{2(aq)}$	266-nm-photolysis of H_2O_2	Resonance fluorescence	1.59 ± 0.32
Sridharan *et al.* [38] (1980)	2−3	295	96% (w/w) $H_2O_{2(aq)}$	discharge of H_2/F_2 with NO_2/H_2O	LIF[b]	1.69 ± 0.26
Keyser *et al.* [39] (1980)	1−4	298	95% (w/w) $H_2O_{2(aq)}$	discharge of H_2 with NO_2	Resonance fluorescence	1.64 ± 0.32

[a] in cm^3 $molecule^{-1}$ s^{-1}

[b] LIF: Laser-induced fluorescence.

C. Line strength measurements of the ν_1 fundamental transitions of OH.

The measurements of the absolute line strength of the OH ν_1 fundamental transitions were carried out by means of synchronized two-color time-resolved dual-comb spectroscopic technique that enables to simultaneously record time-dependent difference absorbance spectra of H_2O_2 and OH radicals. The representative time-resolved dual-comb spectra are shown in Figure 2 and the difference absorbance spectra at specific time after flash photolysis can be extracted from these time-resolved dual-comb spectra for determinations of the integrated difference absorbance areas of the OH and H_2O_2 absorption lines. Figure S5 shows the difference absorbance spectra of H_2O_2 near 1269.64 cm^{-1} obtained at 10–11 ms after laser photolysis of the flowing mixture of H_2O_2/N_2 (0.0145/10.04 Torr, P_T = 10.05 Torr, 296 K). The spectrum was curve-fitted with the multipeak Voigt function to obtain

the integral difference absorbance area of each absorption peak at 10–11 ms after laser photolysis which can be used to derive the temporal profiles of the H_2O_2 integrated difference absorbance area, as shown in Figure 6(a). The profile of H_2O_2 shows an instant consumption due to the UV photodissociation of H_2O_2, followed by a relatively slow decay which is mainly caused by the reaction of OH + H_2O_2. The H_2O_2 time trace thus was fitted with a single-exponential function using a fixed decay time which is corresponding to an inverse of the first-order rate coefficient of the reaction OH + H_2O_2 to obtain the value of integral difference absorbance area at time of zero ($[\text{Int. } \Delta\text{Abs.}]_{H2O2,t=0}$). Considering the error of our measured rate coefficient of the reaction OH + H_2O_2, the derived $[\text{Int. } \Delta\text{Abs.}]_{H2O2,t=0}$ might have an additional uncertainty of ~4%. On the other hand, the integral difference absorbance area of the absorption lines for the initially generated OH radicals ($[\text{Int. } \Delta\text{Abs.}]_{OH,t=0}$) can be derived by analyzing their high-resolution spectra (Figure S6) and temporal profiles (Figure 6(b)). Additionally, herein we assumed that the line strengths for doublet transitions are the same. Adopting the quantum yield of OH from 248-nm photolysis of H_2O_2, line strength of H_2O_2, and the ratio of the integral difference absorbance area of the initially generated OH radicals and that of instant consumption of H_2O_2, we thus estimated the line strength of the selected OH transitions. Figure 7 shows the statistical distribution of 12 measurements of the line strength for one of the $X^2\Pi_{1/2}$ (1←0) P(3.5) doublet transitions. By taking into account the errors of statistical analysis and determined S_{H2O2} as well as the uncertainty of $[\text{Int. } \Delta\text{Abs.}]_{H2O2,t=0}$ induced by the error of the rate coefficient of the reaction OH + H_2O_2, the line strength for one of the $X^2\Pi_{1/2}$ (1←0) P(3.5) doublet transitions was hence determined to be $(1.91\pm0.15)\times10^{-20}$ cm molecule^{-1} which is in agreement but more precise than the value of $(1.9\pm0.6)\times10^{-20}$

obtained in our previous experiments of $HO_2 + NO \rightarrow OH + NO_2$.[17] A comparison of the measured line strengths of the absorption lines of OH with the values tabulated in the HITRAN database is shown in Table 3. Five sets of the doublet transitions of the OH ν_1 fundamental band were evaluated in this work and all experimental conditions and obtained line strengths are listed in Table S3. Overall, our determined absolute line strengths of the OH ν_1 transitions have a small uncertainty of <10% and they are lower than that tabulated in the HITRAN database by a factor of ~1.4. Because current line strengths in the HITRAN database were derived mainly according to the near infrared airglow OH emissions observed from the high-altitude atmosphere with the theoretical simulations, direct line strength measurements of OH radicals under well-controlled experimental conditions achieved in this work might be crucial in improvement of the line strength simulations and updating the HITRAN database. Most importantly, the accurate OH line strengths can be used to precisely quantify the yield or depletion of OH radicals in many key atmospheric reactions and to explore the radical–radical reactions such as the reactions of OH with peroxy radicals.[32,41,42]

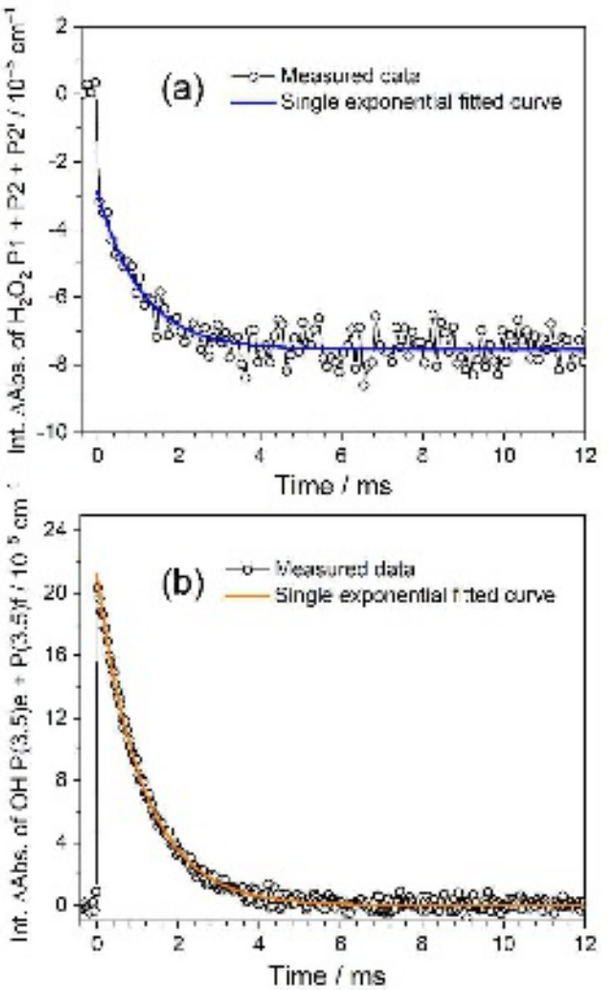

FIGURE 6. Temporal profiles of the summed integrated ΔAbs. of (a) the peaks P1, P2 and P2' of H_2O_2 and (b) two transitions $X^2\Pi_{1/2}$ (1←0) P(3.5)e and P(3.5)f of OH. Each temporal profile was obtained from the time-resolved dual-comb spectra recorded upon photolysis at 248 nm of a flowing mixture of H_2O_2/N_2 (0.0145/10.04 Torr, P_T = 10.05 Torr, 296 K). The blue line represents the single exponential fitted curve with a fixed decay time of 1.08 ms, which is corresponding to $1/(k_{OH+H2O2}\times[H_2O_2]_0)$, where $k_{OH+H2O2}$ is 1.97×10^{-12} cm^3 $molecule^{-1}$ s^{-1} and $[H_2O_2]_0$ is 4.72×10^{14} molecule cm^{-3}. The orange line represents the single exponential fitted curve with a fitted decay time of ~1.12 ms.

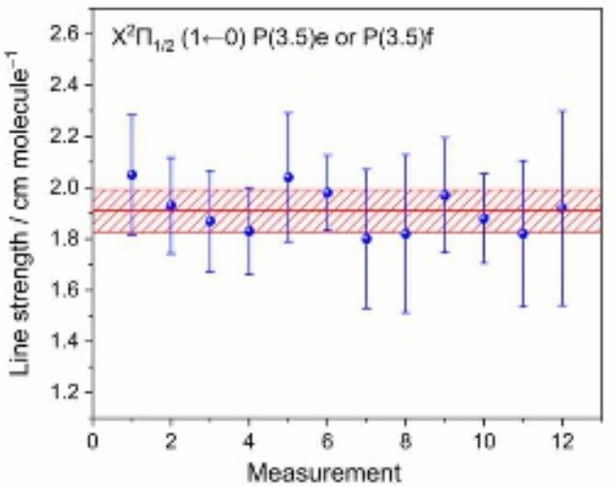

FIGURE 7. Statistical distribution of 12 measurements of the line strength for one of the $X^2\Pi_{1/2}$ (1←0) P(3.5) doublet transitions. The shaded area represents one standard deviation of the 12 measurements.

TABLE 3. Comparison of the obtained line strengths of the OH transitions with the values tabulated in the HITRAN database.

Expt. set	Transition [a]	Line center [a,b]	HITRAN line strength [a,c]	Observed line strength [c]	Difference [d]
1	$X^2\Pi_{1/2}$ (1←0) P(4.5)e	3377.8875	1.54×10^{-20}	$(1.09\pm0.09)\times10^{-20}$	–29.2%
	$X^2\Pi_{1/2}$ (1←0) P(4.5)f	3378.0773	1.54×10^{-20}	$(1.09\pm0.09)\times10^{-20}$	–29.2%
2	$X^2\Pi_{3/2}$ (1←0) P(4.5)f	3407.6117	4.54×10^{-20}	$(3.38\pm0.25)\times10^{-20}$	–25.6%
	$X^2\Pi_{3/2}$ (1←0) P(4.5)e	3407.9885	4.56×10^{-20}	$(3.38\pm0.25)\times10^{-20}$	–25.9%
3	$X^2\Pi_{1/2}$ (1←0) P(3.5)e	3421.9322	2.55×10^{-20}	$(1.91\pm0.15)\times10^{-20}$	–25.1%
	$X^2\Pi_{1/2}$ (1←0) P(3.5)f	3422.0141	2.54×10^{-20}	$(1.91\pm0.15)\times10^{-20}$	–24.8%
4	$X^2\Pi_{1/2}$ (1←0) P(2.5)f	3465.2478	3.14×10^{-20}	$(2.41\pm0.28)\times10^{-20}$	–23.2%
	$X^2\Pi_{1/2}$ (1←0) P(2.5)e	3465.2702	3.14×10^{-20}	$(2.41\pm0.28)\times10^{-20}$	–23.2%
5	$X^2\Pi_{3/2}$ (1←0) P(2.5)f	3484.5983	5.59×10^{-20}	$(4.15\pm0.31)\times10^{-20}$	–26.3%
	$X^2\Pi_{3/2}$ (1←0) P(2.5)e	3484.7482	5.60×10^{-20}	$(4.15\pm0.31)\times10^{-20}$	–25.9%

[a] Line parameters tabulated in the HITRAN database.[21]
[b] Line center in cm^{-1}.
[c] Strength in cm $molecule^{-1}$.
[d] The difference is defined as (observed line strength – HITRAN line strength) / (HITRAN line strength).

IV. CONCLUSIONS

In conclusion, the rate coefficient of the reaction OH + H_2O_2 and the absolute line strength of several ν_1 fundamental transitions of OH have been investigated in detail by employing the mid-infrared two-color time-resolved dual-comb spectrometers. In addition to determining the line strength of a few ν_6 fundamental transitions of H_2O_2 near 7.9 μm in the absence of laser photolysis, we simultaneously recorded the time-resolved spectra of the OH radicals near 2.9 μm upon the 248-nm irradiation of the H_2O_2/N_2 flowing mixtures at varied conditions to explore the kinetics for the reaction OH + H_2O_2. The pressure independent rate coefficient of $[1.97\ (+0.10\ /\ -0.15)] \times 10^{-12}$ cm^3 $molecule^{-1}$ s^{-1} for the reaction of OH with H_2O_2 was obtained under the total pressure of 10.1–55.0 Torr at 296 K. Furthermore, the line strengths of ten OH transitions near 3378, 3408, 3422, 3465, and 3484 cm^{-1} were also measured in this work. Both the accurate rate coefficient $k_{OH+H2O2}$ and line strengths of OH transitions would be important to further revisit the kinetics of the reaction between OH and HO_2 radicals and to resolve the large difference of its rate coefficients between two recent experiments.[12,32] Moreover, the proposed approach with mid-infrared two-color time-resolved dual-comb spectroscopy holds promise for precision measurements of the infrared absorption cross section of transient free radicals and intermediates, as well as for investigations on their self-reaction kinetics.

SUPPLEMENTARY MATERIAL

The supplementary material comprises the UV absorption cross-sections of H_2O_2, the representative OH difference absorbance time trace, plots of the integrated absorbance areas vs. the $[H_2O_2]_0$, plots of k_{obs} vs. $[H_2O_2]_0$ for different experimental sets, the employed kinetic model, difference absorbance spectra of H_2O_2 and OH, and summary of experimental conditions for measurements of the rate coefficient for the reaction OH + H_2O_2 and the OH line strengths.

ACKNOWLEDGMENTS

This project is supported by National Science and Technology Council, Taiwan (grant No. 111-2112-M-001-067 and grant No. 111-2639-M-A49-001-ASP) and Academia Sinica. C. Fittschen and P-L. Luo thank NSTC and MESR for financial support through PHC Orchid project (grant No. 112 -2927-I-001-503).

AUTHOR DECLARATIONS

Conflict of Interest

The authors have no conflicts to disclose.

C.-W. Chang and I-Y. Chen contributed equally to this work.

DATA AVAILABILITY

The data that support the findings of this study are available from the corresponding authors upon reasonable request.

REFERENCES

(1) D. Stone, L. K. Whalley, and D. E. Heard, Chem. Soc. Rev. **41**, 6348 (2012).

(2) B. Franco, T. Blumenstock, C. Cho, L. Clarisse, C. Clerbaux, P.-F. Coheur, M. De Mazière, I. De Smedt, H.-P. Dorn, T. Emmerichs, H. Fuchs, G. Gkatzelis, D. W. T. Griffith, S. Gromov, J. W. Hannigan, F. Hase, T. Hohaus, N. Jones, A. Kerkweg, A. Kiendler-Scharr, E. Lutsch, E. Mahieu, A. Novelli, I. Ortega, C. Paton-Walsh, M. Pommier, A. Pozzer, D. Reimer, S. Rosanka, R. Sander, M. Schneider, K. Strong, R. Tillmann, M. Van Roozendael, L. Vereecken, C. Vigouroux, A. Wahner and D. Taraborrelli, Nature **593**, 233 (2021).

(3) M. Li, E. Karu, C. Brenninkmeijer, H. Fischer, J. Lelieveld, and J. Williams, npj Clim. Atmos. Sci. **1**, 29 (2018).

(4) E. Y. Pfannerstill, N. G. Reijrink, A. Edtbauer, A. Ringsdorf, N. Zannoni, A. Araújo, F. Ditas, B. A. Holanda, M. O. Sá, A. Tsokankunku, D. Walter, S. Wolff, J. V. Lavrič, C. Pöhlker, M. Sörgel, and J. Williams, Atmos. Chem. Phys. **21**, 6231 (2021).

(5) J. Lelieveld, S. Gromov, A. Pozzer, and D. Taraborrelli, Atmos. Chem. Phys. **16**, 12477 (2016).

(6) J. Lelieveld, T. M. Butler, J. N. Crowley, T. J. Dillon, H. Fischer, L. Ganzeveld, H. Harder, M. G. Lawrence, M. Martinez, D. Taraborrelli, and J. Williams, Nature **452**, 737 (2008).

(7) D. Stone, L. K. Whalley, T. Ingham, P. M. Edwards, D. R. Cryer, C. A. Brumby, P. W. Seakins, and D. E. Heard, Atmos. Meas. Tech. **9**, 2827, (2016).

(8) T. Ingham, A. Goddard, L. K. Whalley, K. L. Furneaux, P. M. Edwards, C. P. Seal, D. E. Self, G. P. Johnson, K. A. Read, J. D. Lee, and D. E. Heard, Atmos. Meas. Tech. **2**, 465 (2009).

(9) I. C. Faloona, D. Tan, R. L. Lesher, N. L. Hazen, C. L. Frame, J. B. Simpas, H. Harder, M. Martinez, P. D. Carlo, X. Ren and W. H. Brune, J. Atmos. Chem. **47**, 139 (2004).

(10) D. E. Heard and M. J. Pilling, Chem. Rev. **103**(12), 5163 (2003).

(11) F. A. F. Winiberg, S. C. Smith, I. Bejan, C. A. Brumby, T. Ingham, T. L. Malkin, S. C. Orr, D. E. Heard, and P. W. Seakins, Atmos. Meas. Tech. **8**, 523 (2015).

(12) E. Assaf and C. Fittschen, J. Phys. Chem. A, **120**, 7051 (2016).

(13) A. O. Hui, M. Fradet, M. Okumura, and S. P. Sander, J. Phys. Chem. A, **123**, 3655 (2019).

(14) W. Zhao, B. Fang, X. Lin, Y. Gai, W. Zhang, W. Chen, Z. Chen, H. Zhang, and W. Chen, Anal. Chem., **90**, 3958 (2018).

(15) N. Wei, B. Fang, W. Zhao, C. Wang, N. Yang, W. Zhang, W. Chen, and C. Fittschen, Anal. Chem., **92**, 4334 (2020).

(16) N. Yang, B. Fang, W. Zhao, C. Wang, F. Cheng, X. Hu, Y. Chen, W. Zhang, W. Ma, G. Zhao, and W. Chen, Opt. Express **30**, 15238 (2022).

(17) P.-L. Luo and E.-C. Horng, Commun. Chem. **3**, 95 (2020).

(18) P.-L. Luo and I-Y. Chen, Anal. Chem. **94**, 5752–5759 (2022).

(19) J. S. A. Brooke, P. F. Bernath, C. M. Western, C. Sneden, M. Afşar, G. Li, I. E. Gordon, J. Quant. Spectrosc. Radiat. Transfer, **168**, 142 (2016).

(20) S. Noll, H. Winkler, O. Goussev, and B. Proxauf, Atmos. Chem. Phys., **20**, 5269 (2020).

(21) I. E. Gordon, L. S. Rothman, R. J. Hargreaves, R. Hashemi, E. V. Karlovets, F. M. Skinner, E. K. Conway, C. Hill, R. V. Kochanov, Y. Tan, P. Wcisło, A. A. Finenko, K. Nelson, P. F. Bernath, M. Birk, V. Boudon, A. Campargue, K. V. Chance, A. Coustenis, B. J. Drouin, J.–M. Flaud, R. R. Gamache, J. T. Hodges, D. Jacquemart, E. J. Mlawer, A. V. Nikitin, V. I. Perevalov, M. Rotger, J. Tennyson, G. C. Toon, H. Tran, V. G. Tyuterev, E. M. Adkins, A. Baker, A. Barbe, E. Canè, A. G. Császár, A. Dudaryonok, O. Egorov, A. J. Fleisher, H. Fleurbaey, A. Foltynowicz, T. Furtenbacher, J. J. Harrison, J.–M. Hartmann, V.–M. Horneman, X. Huang, T. Karman, J. Karns, S. Kassi, I. Kleiner, V. Kofman, F. Kwabia–Tchana, N. N. Lavrentieva, T. J. Lee, D. A. Long, A. A. Lukashevskaya, O. M. Lyulin, V. Yu. Makhnev, W. Matt, S. T. Massie, M. Melosso, S. N. Mikhailenko, D. Mondelain, H. S. P. Müller, O. V. Naumenko, A. Perrin, O. L. Polyansky, E. Raddaoui, P. L. Raston, Z. D. Reed, M. Rey, C. Richard, R. Tóbiás, I. Sadiek, D. W. Schwenke, E. Starikova, K. Sung, F. Tamassia, S. A. Tashkun, J. Vander Auwera, I. A. Vasilenko, A. A. Vigasin, G. L. Villanueva, B. Vispoel, G. Wagner, A. Yachmenev, S. N. Yurchenko, J. Quant. Spectrosc. Radiat. Transfer, **277**, 107949 (2022).

(22) J. B. Burkholder, S. P. Sander, J. Abbatt, J. R. Barker, C. Cappa, J. D. Crounse, T. S. Dibble, R. E. Huie, C. E. Kolb, M. J. Kurylo, V. L. Orkin, C. J. Percival, D. M. Wilmouth, and P. H. Wine, *Chemical Kinetics and Photochemical Data for Use in Atmospheric Studies, Evaluation No. 19* (JPL Publication 19-5, Jet Propulsion Laboratory, Pasadena, 2019). http://jpldataeval.jpl.nasa.gov

(23) J. Thiebaud, A. Aluculesei, and C. Fittschen, J. Chem. Phys. **126**, 186101 (2007).

(24) P.-L. Luo, E.-C. Horng, and Y.-C. Guan, Phys. Chem. Chem. Phys., **21**, 18400 (2019).

(25) P.-L. Luo, Opt. Lett., **45**, 6791 (2020).

(26) C.-L. Lin, N. K. Rohatgi, and W. B. DeMore, Geophys. Res. Lett. **5**, 113 (1978).

(27) L. T. Molina and M. J. Molina, J. Photochem. **15**, 97 (1981).

(28) J. M. Nicovich and P. H. Wine, J. Geophys. Res. **93**, 2417 (1988).

(29) G. L. Vaghjiani and A. R. Ravishankara, J. Geophys. Res. **94**, 3487 (1989).

(30) S. Klee, M. Winnewisser, A. Perrin, and J. Flaud, J. Mol. Spectrosc. **195**, 154 (1999).

(31) L. S. Rothman, I. E. Gordon, A. Barbe, D. Chris Benner, P. F. Bernath, M. Birk, V. Boudon, L. R. Brown, A. Campargue, J.-P. Champion, K. Chance, L. H. Coudert, V. Dana, V. M. Devi, S. Fally, J.-M. Flaud, R. R. Gamache, A. Goldman, D. Jacquemart, I. Kleiner, N. Lacome, W. J. Lafferty, J.-Y. Mandin, S. T. Massie, S. N. Mikhailenko, C. E. Miller, N. Moazzen-Ahmadi, O. V. Naumenko, A. V. Nikitin, J. Orphal, V. I. Perevalov, A. Perrin, A. Predoi-Cross, C. P. Rinsland, M. Rotger, M. Šimečková, M. A. H. Smith, K. Sung, S. A. Tashkun, J. Tennyson, R. A. Toth , A. C. Vandaele, J. Vander Auwera, J. Quant. Spectrosc. Radiat. Transfer, **110**, 533–572 (2009).

(32) T. H. Speak, M. A. Blitz, D. J. Medeiros, and P. W. Seakins, JACS Au, **3**(6), 1684 (2023).

(33) http://iupac.pole-ether.fr

(34) G. L. Vaghjiani, A. R. Ravishankara, and N. Cohen, J. Phys. Chem. **93**, 7833 (1989).

(35) M. J. Kurylo, J. L. Murphy, G. S. Haller, and K. D. Cornett, Int. J. Chem. Kinet. **14**, 1149 (1982).

(36) W. J. Marinelli and H. S. Johnston, J. Chem. Phys. **77**, 1225 (1982).

(37) P. H. Wine, D. H. Semmes, and A. R. Ravishankara, J. Phys. Chem. **75**, 4390 (1981).
(38) U. C. Sridharan, B. Reimann, and F. Kaufman, J. Chem. Phys. **73**, 1286 (1980).
(39) L. F. Keyser, J. Phys. Chem. **84**, 1659 (1980).
(40) E. Jiménez, T. Gierczak, H. Stark, J. B. Burkholder, and A. R. Ravishankara, J. Phys. Chem. A, **108**, 1139 (2004).
(41) R. L. Caravan, M. A. H. Khan, J. Zádor, L. Sheps, I. O. Antonov, B. Rotavera, K. Ramasesha, K. Au, M.-W. Chen, D. Rösch, D. L. Osborn, C. Fittschen, C. Schoemaecker, M. Duncianu, A. Grira, S. Dusanter, A. Tomas, C. J. Percival, D. E. Shallcross and C. A. Taatjes, Nat. Commun. **9**, 4343 (2018).
(42) C. Fittschen, Chem. Phys. Lett. **725**, 102 (2019).